Chemical Science

Accepted Manuscript

ROYAL SOCIETY OF CHEMISTRY

rsc.li/chemical-science

View Article Online
DOI: 10.1039/C7SC02693E

Journal Name

ARTICLE

Preferential targeting of I-motifs and G-quadruplexes by small molecules

Received 00th January 20xx,
Accepted 00th January 20xx

DOI: 10.1039/x0xx00000x

www.rsc.org/

Manish Debnath,[a] Shirsendu Ghosh,[b] Ajay Chauhan,[a] Rakesh Paul,[a] Kankan Bhattacharyya[b] and Jyotirmayee Dash[a]*

I-motifs and G-quadruplexes are dynamic nucleic acid secondary structures, which are believed to play key roles in gene expression. We herein report two peptidomimetic ligands (**PBP1** and **PBP2**) that selectively target i-motifs and G-quadruplexes over double-stranded DNA. These peptidomimetics, regioisomeric with respect to the position of triazole/prolinamide motifs have been synthesized using a modular method involving Cu(I)-catalyzed azide and alkyne cycloaddition. The *para*-isomer, **PBP1** exhibits high selectivity for i-motifs while the *meta*-isomer **PBP2** binds selectively to G-quadruplex structures. Interestingly, these ligands have the ability to induce the G-quadruplex or i-motif structures from the unstructured single-stranded DNA conformations as observed by single molecule Förster resonance energy transfer (smFRET) studies. The quantitative real-time polymerase chain reaction (qRT-PCR), western blot and dual-luciferase assays indicate that **PBP1** upregulate and **PBP2** downregulate *BCL-2* gene expression in cancer cells.

Introduction

Cytosine (C)-rich and guanine (G)-rich sequences can adopt stable nucleic acid secondary structures such as i-motifs[1] and G-quadruplexes,[2] respectively. The C-rich sequences form i-motif structures at acidic pH,[3-6] whereas the G-rich sequences usually form G-quadruplexes at neutral pH in the presence of metal ions (Na^+, K^+). These sequences are prevalent in the promoter region of oncogenes like *BCL-2* and *c-MYC*.[7-10] It has been reported that small molecules bind G-quadruplexes[11] and modulate the gene expression.[12-17] Although i-motifs are hypothesized to play important role in gene transcription,[18-21] only a few ligands are known to selectively target i-motifs in biological system.[18-22] Furthermore, i-motifs and G-quadruplexes are highly dynamic and they can exist in equilibrium with unfolded DNA under physiological conditions.[12,18-20] However, little is known about how small molecules can regulate the relative populations of these two dynamic secondary structures. In this context, we envisioned to develop small molecules that can discriminate between i-motif and G-quadruplex structures and modulate gene expression.

The single molecule Förster resonance energy transfer (smFRET) technique provides key information about the structure, relative population distribution of folded or unfolded species and the end-to-end distance of bio-molecules.[23-34] The smFRET has been used to elucidate the conformational dynamics of G-quadruplexes in the presence of metal ions (K^+/Na^+),[28] protein[33] and small molecules.[34] The population equilibrium of C-rich ILPR and *BCL-2* promoter sequences has been studied using laser tweezer experiments.[35,36] Majima and co-workers have used smFRET to quantitatively analyse the pH-induced intra-molecular folding dynamics of an i-motif DNA.[37] However, the use of smFRET to monitor the ligand induced change in relative population distribution of i-motif and G-quadruplex structures present in oncogenic promoters is very limited.

Hurley and Hecht have reported that a steroid ligand **IMC-48** folds the *BCL-2* C-rich sequence to an i-motif, while the same sequence is folded into a hairpin duplex in the presence of a related ligand **IMC-76**.[18,19] In this study, we describe the synthesis of two flexible peptidomimetic congeners **PBP1** and **PBP2** that show structure-specific recognition for G-quadruplex and i-motif structures. The interaction of these ligands with *BCL-2* or *c-MYC* i-motifs and G-quadruplexes has been evaluated using biophysical studies like melting analysis by Förster resonance energy transfer (FRET), thiazole-orange (TO) displacement assay, Fluorescence quenching assay and Circular dichroism (CD) spectroscopy. In addition, the ability of these ligands to induce the formation of i-motif and G-quadruplex structures from the unfolded *BCL-2* and *c-MYC* C-rich and G-rich promoter sequences has been investigated

[a] Department of Organic Chemistry, Indian Association for the Cultivation of Science, Jadavpur, Kolkata-700032, India.
[b] Department of Physical Chemistry, Indian Association for the Cultivation of Science, Jadavpur, Kolkata-700032, India.
Electronic Supplementary Information (ESI) available: [Experimental details, synthetic procedures, characterization data of compounds, ^{1}H NMR and ^{13}C NMR spectra, FRET melting, TO displacement, smFRET, lifetime data, CD spectra, western blot, dual luciferase, caspase assay. See DOI: 10.1039/x0xx00000x

View Article Online
DOI: 10.1039/C7SC02693E

using smFRET and fluorescence lifetime studies at neutral pH. We have further demonstrated how ligand-dependent conformational changes of *BCL-2* i-motif or G-quadruplex topologies can modulate the *BCL-2* expression in cancer cells.

Results and discussion

Design and synthesis of peptidomimetic ligands

Peptidomimetics are designed to interact with specific biological targets as they exhibit enhanced proteolytic stability and improved cell permeability.[38,39] We have anticipated that peptidomimetics containing 2, 6-pyridine dicarboxamide unit, linked to L-proline residues through triazole and arene motifs would be structurally flexible to adopt different conformations upon interacting with different DNA four stranded structures (i-motifs and G-quadruplexes). The proline residues play an important role in peptide conformation. The 2, 6-pyridine dicarboxamide motif can adopt folded conformations due to the bifurcated H-bonding between the lone pair of pyridine nitrogen and amide –NH protons. The arene motif attached with the proline residues would provide additional flexibility to form topologically different positional isomers that could discriminate different DNA structures such as i-motifs and G-quadruplexes (Fig. S1, Supporting Information, ESI). And further, the triazole ring system could facilitate stacking interaction with the loop bases and thus, could differentially interact with different DNA secondary structures with variations in loop region.[40] The triazole ring system, able to mimic the *cis*- or *trans*- conformations of amide bonds would impart rigidity to the peptidomimetics. It has been reported that triazole containing ligands, generated by "click" chemistry selectively bind G-quadruplexes.[41-43]

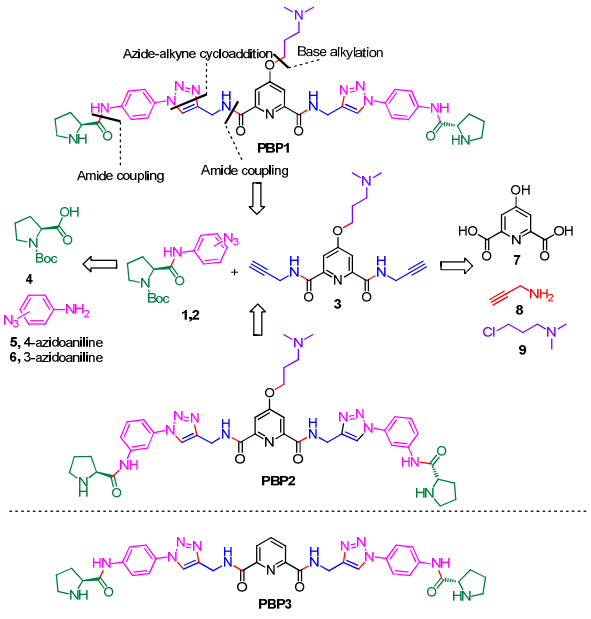

Scheme 1 Synthesis of bis-prolinamide derivatives **PBP1**, **PBP2** and structure of **PBP3.**

The bis-triazole containing peptidomimetic type ligands **PBP1** and **PBP2** were assembled using a modular synthetic strategy involving a Cu(I)-catalyzed 1, 3-dipolar azide-alkyne cycloaddition between azido prolinamides **1**, **2** and pyridyl dialkyne **3** (Scheme 1, Scheme S1, ESI). The azido prolinamides **1** and **2** were obtained by amide coupling of N-Bocproline **4** with the *para* and *meta*-azido anilines **5** and **6**. The dialkyne building block **3** was prepared from cheledamic acid **7**. Cheledamic acid **7** was treated with oxalyl chloride to generate the corresponding acid chloride, which was subsequently coupled with propargyl amine **8**, followed by alkylation of the resulting pyridyl dialkyne with 3-dimethylaminopropyl chloride **9** afforded the dialkyne **3** in high overall yield. The Cu(I)-catalyzed Huisgen cycloaddition of azido prolinamide derivatives **1** and **2** with the dialkyne **3** and subsequent removal of the Boc group provided the bis-prolinamide derivatives **PBP1** and **PBP2** in high yields. The bis-prolinamide derivative **PBP3** was similarly assembled from azido prolinamide **1** and pyridine-2, 6-dicarboxylic acid.

PBP1 and PBP2 exhibit differential binding between i-motifs and G-quadruplexes

The ability of these regioisomeric ligands to interact with G-quadruplexes and i-motifs was evaluated by biophysical assays. C-rich sequences were folded into i-motifs by annealing in 60 mM K-cacodylate buffer, pH 4.8 and the pH was adjusted to 6 for biophysical analysis.[18,22,44,45]

(a) Melting analysis by FRET. FRET based melting assay was carried out to evaluate the stabilization potential of **PBP 1-3** for G-quadruplexes and i-motifs.[46,47] Dual labeled (5'-FAM and 3'-TAMRA) C-rich and G-rich sequences, present in oncogenic promoter regions (*BCL-2* and *c-MYC*) and telomeric region (*h-TELO*) were folded into i-motifs and G-quadruplexes, respectively[18,48] and they were used in this study along with a control double-stranded (*ds*) DNA (Fig. 1 and Table S1, ESI).

Interestingly, the two positional isomers **PBP1** and **PBP2** exhibited a marked difference in increasing the T_m of folded G-quadruplexes and i-motifs at 1 μM ligand concentration (Table 1, Fig. 1a, 1b and Fig. S2, ESI). Ligand **PBP1**, in which the prolinamide motifs are at the *para* position with respect to the triazole ring system, increased the T_m values of *BCL-2*-C and *c-MYC*-C i-motifs more effectively compared to ligand **PBP2** at 1 μM ligand concentration (ΔT_m = 16-29 °C for **PBP1** and ΔT_m = 8 °C for **PBP2**). In contrast, the *meta* regioisomer, **PBP2** increased the ΔT_m value of *c-MYC*-G and *BCL-2*-G G-quadruplexes (ΔT_m = 16 °C at 1 μM **PBP2** and ΔT_m = 5.2 °C at 1 μM **PBP1**) (Table 1). Ligand **PBP3** that lacks the $-NMe_2$ side chain in the central pyridine ring showed low stabilization potential (ΔT_m = 3-5 °C) for both G-quadruplex and i-motif structures (Table S1, ESI). When *BCL-2*-C and *c-MYC*-C mutant C-rich sequences were used in the melting analysis, no melting curves were observed thereby indicating their existence in unfolded form (Fig. S3, ESI).

View Article Online
DOI: 10.1039/C7SC02693E

Table 1. Sequences used in this study and comparison of binding data obtained for **PBP1** and **PBP2** from TO displacement, fluorescence quenching and FRET melting assay.

DNA[a]	DC_{50} (μM)[b]		K_d (μM)[c]		ΔT_m[d] (°C)	
	PBP1	PBP2	PBP1	PBP2	PBP1	PBP2
BCL-2-C: 5′-d(CAGC$_4$GCTC$_3$GC$_5$T$_2$C$_2$TC$_3$GCGC$_3$GC$_4$T)-3′	0.9	8.2	0.3	5.8	29	8
BCL-2-G: 5′-d(AG$_4$CG$_3$CGCG$_3$AG$_2$A$_2$G$_5$CG$_3$AGCG$_4$CGT)-3′	5.7	2.4	7.2	1.9	5.2	16
c-MYC-C: 5′-d(TC$_4$AC$_2$T$_2$C$_4$AC$_3$TC$_4$AC$_3$TC$_4$A)-3′	2.7	6.8	2.4	9.5	16	8
c-MYC-G: 5′-d(TG$_4$AG$_3$TG$_4$AG$_3$TG$_4$A$_2$G$_2$TG$_4$A)-3′	8.5	1.3	12.5	1.3	5.2	16
h-TELO-C: 5′-d(TA$_2$C$_3$TA$_2$C$_3$TA$_2$C$_3$TA$_2$C$_3$)-3′	4	>15	n.d.	n.d.	9	5
h-TELO-G: 5′-d(G$_3$TTAG$_3$TTAG$_3$TTAG$_3$)-3′	9.8	4.7	n.d.	n.d.	5	8
ds DNA: 5′-d(TATAGCTATA-HEG-TATAGCTATA)-3′	n.d.	n.d.	>25	>25	0.94	1.1

[a]Unlabeled, single TAMRA labeled and dual FAM-TAMRA labeled sequences were used in TO displacement, fluorescence quenching and FRET melting experiments, respectively; HEG = Hexaethylene glycol.

[b]Error = ± 5 %;

[c]K_d values indicated for the 5′-labeled sequences (K_d = ± 5 %). **PBP1** (fold selectivity): *BCL-2*-C/*c-MYC*-C/*BCL-2*-G/*c-MYC*-G = 40/6/1.5/1; **PBP2** (fold selectivity): *BCL-2*-C/*c-MYC*-C/*BCL-2*-G/*c-MYC*-G = 1.5/1/ 4.5/7;

[d]ΔT_m = ±1 °C; [**PBP1**] = [**PBP2**] = 1 μM; The T_m values of folded *c-MYC*-C, *BCL-2*-C, *h-TELO*-C i-motifs and *ds* DNA diluted in 60 mM K-cacodylate buffer, pH 6 are 48 ± 1 °C, 59 ± 1 °C, 43 ± 1 °C and 60 ± 1 °C (Table S1, ESI). The T_m values of folded *c-MYC*-G, *BCL-2*-G and *h-TELO*-G diluted in 60 mM K-cacodylate buffer, pH 7 are 69 ± 1 °C, 70 ± 1 °C, 55 ± 1 °C.

Next, FRET melting experiments were carried out for *BCL-2*, *c-MYC* and *h-TELO* i-motifs and G-quadruplexes using increasing concentration of **PBP 1-2**. **PBP1** showed high ΔT_m values for *BCL-2*-C, *c-MYC*-C and *h-TELO*-C i-motifs while **PBP2** exhibited high ΔT_m values for the corresponding G-quadruplexes in a dose-dependent manner (Fig. 1c, 1d, Fig. S2-S4, ESI). **PBP1** showed a ΔT_m value of 32 ± 1 °C (i.e., a T_m of 92 °C) for *BCL-2*-C at 1.3 μM concentration, whereas higher concentrations of **PBP1** were required to attain a ΔT_m value of 32 ± 1 °C for *c-MYC*-C (a T_m of 81 °C at 6.5 μM) and *h-TELO*-C (a T_m of 76 °C at 10 μM). These results indicate that **PBP1** shows a preferential affinity for *BCL-2*-C i-motif as it can attain maximum ΔT_m value for *BCL-2*-C i-motif at 5-8 fold lower concentrations compared to *c-MYC*-C and *h-TELO*-C i-motifs. In contrast, *BCL-2*-G and *c-MYC*-G G-quadruplexes exhibited maximum ΔT_m values at 3 fold lower concentrations of **PBP2** over **PBP1** (Fig. S2, ESI). However, both **PBP1** and **PBP2** failed to alter the T_m of *ds* DNA even at high ligand concentrations (10-15 μM) indicating their selectivity for four stranded structures over double-stranded DNA.

The selectivity of **PBP1** for i-motifs and **PBP2** for G-quadruplexes was determined by using FRET competition assay with competitors G-quadruplex $(TG_5T)_4$ and double-stranded ds26 DNA (Fig. S2c and S2d, ESI). The results show that no significant changes in the ΔT_m values of **PBP1** bound i-motifs and **PBP2** bound G-quadruplexes were observed in the presence of 40 mol equivalent excess of G-quadruplex and double-stranded DNA competitors.

(b) TO displacement assay. The affinity of **PBP 1-3** for the folded G-quadruplexes and i-motifs were further investigated by measuring the ability of the ligands to displace the bound thiazole-orange (TO) from pre-folded G-quadruplexes[49] or i-motifs[50] (Fig. 1e and 1f). Table S2 lists the concentrations of the ligands required to displace TO by 50 % (DC_{50}) from the investigated DNA structures.

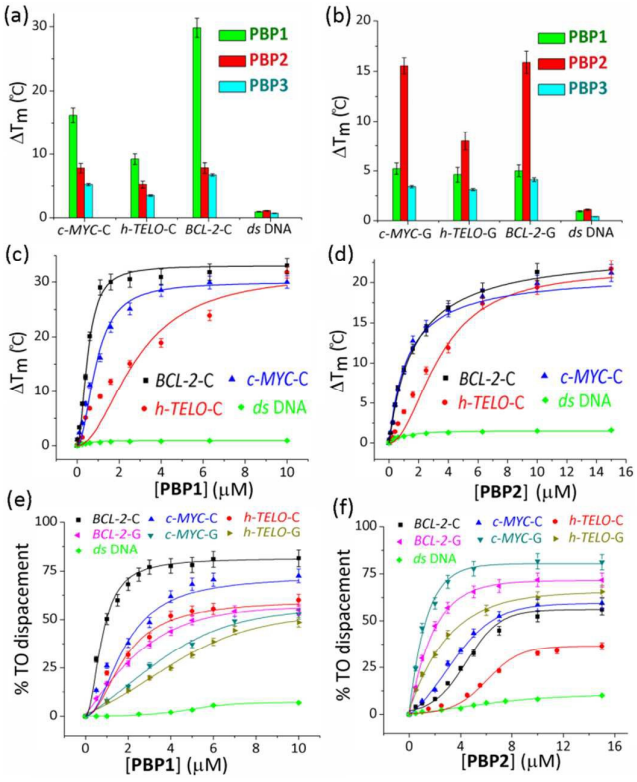

Fig. 1 FRET melting and TO displacement assay. FRET stabilization potential of bis-prolinamide derivatives **PBP1** (1 μM), **PBP2** (1 μM) and **PBP3** (1 μM) upon interaction with (a) 100 nM folded i-motifs (*c-MYC*-C, *BCL-2*-C, *h-TELO*-C) and *ds* DNA in 60 mM K-cacodylate buffer, (pH 6); (b) 100 nM folded G-quadruplexes (*c-MYC*-G, *BCL-2*-G, *h-TELO*-G) and *ds* DNA in 60 mM K-cacodylate buffer, (pH 7); Thermal shift profiles for (c) **PBP1** (0-10 μM) and (d) **PBP2** (0-15 μM) upon stabilizing i-motifs and *ds* DNA in 60 mM K-cacodylate buffer, (pH 6). TO displacement from 250 nM *BCL-2*-C, *c-MYC*-C, *h-TELO*-C i-motifs in 60 mM K-cacodylate buffer, (pH 6); *BCL-2*-G, *c-MYC*-G, *h-TELO*-G G-quadruplexes and *ds* DNA in 60 mM K-cacodylate buffer, (pH 7) with increasing concentrations of (e) **PBP1** (0-10 μM); (f) **PBP2** (0-15 μM).

View Article Online
DOI: 10.1039/C7SC02693E

PBP1 exhibited DC_{50} values of 0.9 μM, 2.7 μM and 4.0 μM for *BCL-2*-C, *c-MYC*-C and *h-TELO*-C i-motifs, respectively (Table 1). In comparison, the *meta*-isomer **PBP2** displayed significantly lower affinity for *BCL-2*-C (DC_{50} = 8.2 μM), *c-MYC*-C (DC_{50} = 6.8 μM) and *h-TELO*-C (DC_{50} >15 μM) i-motifs. On the other hand, **PBP1** showed higher DC_{50} values for *BCL-2*-G, *c-MYC*-G and *h-TELO*-G G-quadruplexes compared to **PBP2** (Table 1). These results are in agreement with the FRET melting data suggesting higher affinity of **PBP1** for *BCL-2*-C i-motif as compared to **PBP2** and preferential binding of **PBP2** for *c-MYC*-G and *BCL-2*-G G-quadruplexes as compared to **PBP1.** However, ligand **PBP3** exhibited high DC_{50} values for G-quadruplexes (DC_{50} = 8.4-10.2 μM) and i-motifs (DC_{50} = 7.9-10 μM), which indicates weak affinity of **PBP3** for both four stranded structures (Fig. S5, ESI).

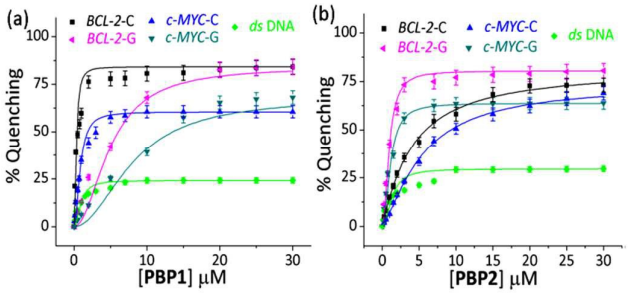

Fig. 2 The percentage fluorescence quenching observed upon titration of 250 nM of 5′-TAMRA labeled folded *BCL-2*-C and *c-MYC*-C i-motif structures in 60 mM K-cacodylate buffer, (pH 6) and 250 nM 5′-TAMRA labeled folded *BCL-2*-G and *c-MYC*-G G-quadruplex structures in 60 mM K-cacodylate buffer, (pH 7) by (a) 0-30 μM **PBP1**; (b) 0-30 μM **PBP2**.

(c) Fluorescence binding titrations. Next, fluorescence spectroscopy was employed to determine the binding dissociation constants (K_d) of **PBP1** and **PBP2** with *BCL-2* and *c-MYC* i-motifs and G-quadruplexes (Table S3 and S4, ESI). Here, i-motifs and G-quadruplexes are labeled at either 5′-end or at 3′-end with TAMRA dye. Binding of the ligand in the vicinity of the labeled site facilitates proximity induced quenching of the dye through non radiative methods (Scheme S2, ESI).[51] For a comparison, *ds* DNA was used as a control. We observed a dose-dependent decrease in the fluorescence emission of TAMRA labeled DNA structures upon titration with **PBP1** and **PBP2** (Fig. 2 and S6, ESI). From the level of quenching, K_d values of the ligands for the i-motif and G-quadruplex structures were determined. **PBP1** showed a 20 fold higher affinity for 5′-TAMRA-*BCL-2*-C i-motif with a K_d value of 0.3 μM over **PBP2** (K_d = 5.8 μM) (Table 1). Similarly, **PBP1** exhibited lower K_d value (2.4 μM) for 5′-TAMRA-*c-MYC*-C i-motif compared to **PBP2** (K_d = 9.5 μM).

When 5′-TAMRA labeled *BCL-2*-G and *c-MYC*-G G-quadruplexes were titrated with **PBP1** and **PBP2,** a marked difference in their affinity was observed. **PBP2** exhibited a 7 fold preference for 5′-labeled *c-MYC*-G (K_d = 1.3 μM) G-quadruplex over the i-motif counterpart. Similarly, a 3 fold higher affinity of **PBP2** was observed for *BCL-2*-G G-quadruplex (K_d = 1.9 μM) over *BCL-2*-C i-motif. It is intriguing to note that **PBP1** showed a 24 fold selectivity for *BCL-2*-C i-motif over *BCL-2*-G (K_d = 7.2 μM) and a 40 fold selectivity for *BCL-2*-C i-motif over *c-MYC*-G (K_d = 12.5 μM) G-quadruplexes. To the best of our knowledge, this is one of the highest levels of selectivity reported by a small molecule ligand for i-motif over G-quadruplex structures.

Similar binding titrations with 3′-TAMRA labeled *BCL-2* and *c-MYC* i-motifs and G-quadruplexes revealed that both **PBP1** and **PBP2** displayed higher affinity (lower K_d value) for 5′-labeled G-quadruplexes and i-motifs over 3′-labeled structures (Fig. S6, Scheme S2, Table S3 and S4, ESI). Therefore, the 5′-end of G-quadruplex and i-motif structures is the preferential binding site for **PBP1** and **PBP2**. In comparison, **PBP3** induced considerably lower level of fluorescence quenching (>40 %) in TAMRA labeled G-quadruplexes and i-motifs (Fig. S7, ESI), suggesting weak affinity of **PBP3** for these DNA structures. The weak affinity of **PBP3** may be attributed to its poor solubility in aqueous buffer and the lack of cationic side chain and hence **PBP3** was not selected for further studies. Importantly, **PBP1** and **PBP2** preferentially binds to the four stranded DNA structures over *ds* DNA, as control experiments with TAMRA labeled *ds* DNA showed no significant quenching upon addition of ligands (Fig. 2 and S6, ESI).

PBP1 and PBP2 induce the formation of i-motifs and G-quadruplexes, respectively

(a) SmFRET analysis. The smFRET was used to study the conformational changes of folded and free i-motif and G-quadruplex forming sequences in the presence and absence of ligands by monitoring the FRET between donor and acceptor fluorophores. Dual labeled sequences of highest purity (Table S1, ESI) were used to exclude the signals from the donor only sample and further, the donor shot noise contributions were found to be negligible (Table S5, ESI).[34] We observed that the donor-acceptor fluorescence intensities of the dual labeled *BCL-2*-C and *c-MYC*-C i-motif sequences produced anti-correlated fluctuations (Fig. 3 and S8, ESI). The FRET histograms obtained from the time traces were fitted with bi- and single Gaussian distribution. The FRET histogram of *BCL-2*-C i-motif, at pH 4.8, showed a narrow distribution with a mean ε_{FRET} ~ 0.95 (Fig. 3). Using equation S5, the distance (R_{DA}) between the donor and acceptor dyes of *BCL-2*-C i-motif was determined to be ~ 33.7 Å (Table S6, ESI) and thereby indicating the existence of a compact structure. The single narrow distribution *BCL-2*-C i-motif was preserved even after the addition of **PBP1** and **PBP2** (1 equiv.) (Fig. S9, ESI). The pre-folded *BCL-2*-C i-motif, at pH 6 also exhibited a high ε_{FRET} value (~ 0.88) with a correspondingly low R_{DA} ~ 39 Å, suggesting the presence of folded i-motif structures (Fig. S10, ESI). The FRET histogram of the free *BCL-2*-C i-motif sequence at pH 7 showed two population distributions, a wide distribution with FRET efficiency (ε_{FRET}) centered at ~ 0.64 (91 %) and a narrow distribution centered at ε_{FRET} ~ 0.45 (Fig. 3). The distribution with ε_{FRET} ~ 0.45 was ignored due to the contribution of shot noise (Table S5, ESI). The lower ε_{FRET} ~ 0.64 value with a large R_{DA} (~ 50 Å) suggests that the free *BCL-2*-C sequence remains in the unstructured form at pH 7. Upon addition of **PBP1** (1 equiv.), the histogram of the free *BCL-2*-C sequence (pH 7) was

View Article Online
DOI: 10.1039/C7SC02693E

shifted to higher value (ε_{FRET} ~ 0.9) with a R_{DA} of ~ 36.6 Å, which suggests that **PBP1** induces folding of free C-rich sequences into i-motif structures at pH 7. However, **PBP2** (1 equiv.) induces only a partial shift in the population distributions of the free i-motif sequence at pH 7, exhibiting two major populations with ε_{FRET} values of ~ 0.67 (R_{DA} ~ 49 Å) and ~ 0.95 (R_{DA} ~ 33.7 Å). The mutant *BCL-2*-C C-rich sequence exists in an unstructured form showing low FRET efficiencies (~ 57 %) in both Milli-Q water (pH 7) and in 10 mM Na-cacodylate buffer (pH 4.8) (R_{DA} ~ 53 Å) (Fig. 3).

The FRET histogram of the free *c-MYC*-C i-motif sequence at pH 7 showed two major population distributions having mean ε_{FRET} values of ~ 0.55 and ~ 0.8 with R_{DA} ~ 53.2 Å and ~ 43.7 Å, respectively (Fig. S8, ESI). Upon addition of **PBP1** (1 equiv.), the ε_{FRET} distribution was shifted towards higher value (ε_{FRET} ~ 0.95) with a low R_{DA} value of ~ 33.7 Å, indicating **PBP2** (~ 0.93) (R_{DA} ~ 35.7 Å), indicating the formation of a compact i-motif structure; whereas **PBP2** (1 equiv.) did not significantly alter the FRET distribution pattern of the free *c-MYC*-C i-motif sequence at pH 7. Similar to *BCL-2*-C i-motif, the folded *c-MYC*-C i-motif at pH 4.8 showed a single population with mean ε_{FRET} value ~ 0.95, indicating the formation of a more compact structure with lower end-to-end distances (R_{DA} ~ 33.7 Å).

Similar to the folded i-motifs, the folded G-quadruplexes are known to exhibit lower R_{DA} values compared to unstructured G-rich sequences.[34] The free *BCL-2*-G G-quadruplex sequence showed a wide distribution centered at ε_{FRET} ~ 0.6 with a corresponding R_{DA} of ~ 51.4 Å (Fig. S11a and S11b, ESI). **PBP2** (1 equiv.) could significantly shift the populations of free *BCL-2*-G sequence towards higher value

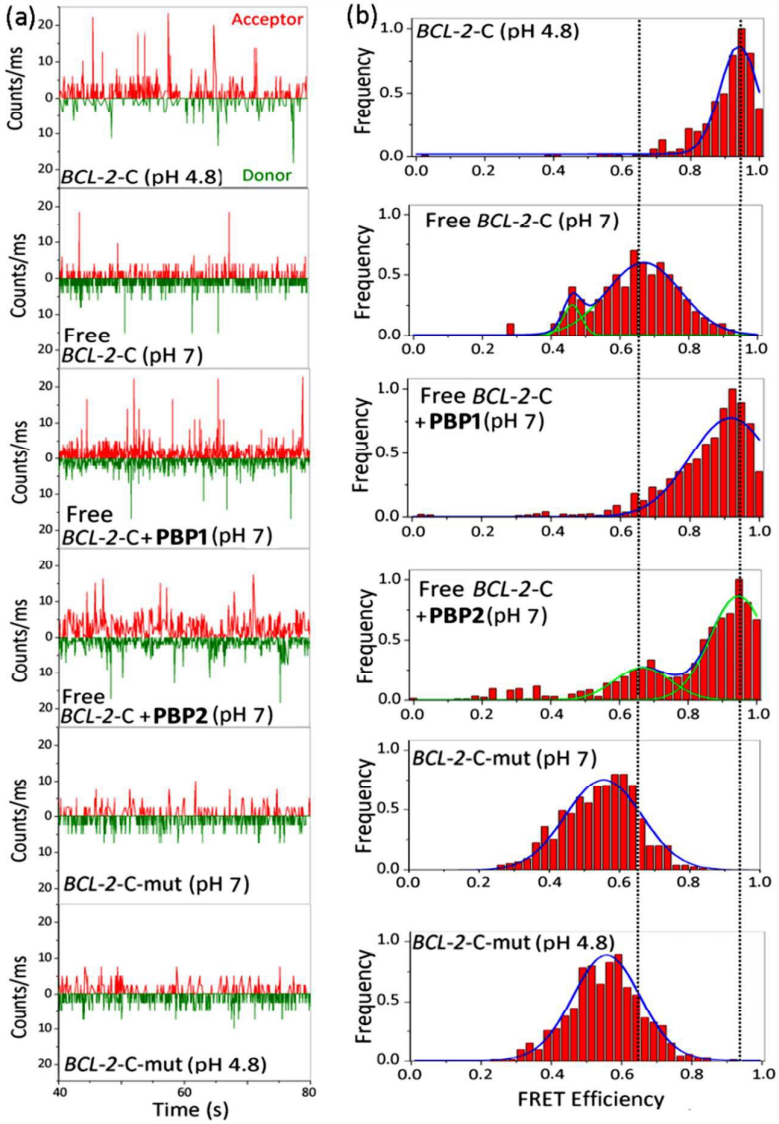

Fig. 3 The smFRET analysis of *BCL-2*-C and mutated *BCL-2*-C (*BCL-2*-C-mut). Photon bursts of donor/acceptor (background corrected) (a); and FRET efficiency distributions (b); of 100 pM dual fluorescently labeled *BCL-2*-C and *BCL-2*-C-mut at neutral (pH 7) and acidic (pH 4.8) conditions or in the presence of **PBP1** (1 equiv.), **PBP2** (1 equiv.). *BCL-2*-C-mut: 5'- FAM-d($CAGC_2TCGCTC_2TGC_2TC_2T_2C_2TC_2TGCGC_2TGC_2TCG$)-TAMRA-3'.

View Article Online
DOI: 10.1039/C7SC02693E

could induce a compact G-quadruplex structure similar to the K^+-folded G-quadruplex.[34] On the other hand, the free *BCL-2*-G sequence showed two major populations with ε_{FRET} values of ~ 0.6 (R_{DA} ~ 51.4 Å) and ~ 0.85 (R_{DA} ~ 41.2 Å) in the presence **PBP1** (1 equiv.). The addition of **PBP2** decreased the R_{DA} value of free *c-MYC*-G from ~ 57 Å to ~ 41 Å in the absence of K^+ ions (Fig. S11c, S11d and Table S6, ESI). However, the non-G-quadruplex forming mutated *BCL-2*-G sequence did not exhibit any notable change in ε_{FRET} values upon addition of ligands **PBP1** and **PBP2** (ε_{FRET} ~ 0.6), suggesting that the mutated sequences are unstructured even in the presence of the ligands (Fig. S12, ESI).

Collectively, the smFRET results suggest that ligand **PBP1** can completely shift the dynamic equilibrium of C-rich *BCL-2*-C and *c-MYC*-C sequences towards the folded i-motifs from the unstructured form at physiologically relevant neutral pH conditions. However, **PBP2** induces only a partial shift in the population distributions of free i-motif sequences at neutral pH but it has the ability to trigger the formation of G-quadruplexes from the unstructured G-rich sequences in the absence of K^+ ion.

(b) Fluorescence lifetime analysis. The differential folding behaviour of free *c-MYC*-C and *BCL-2*-C i-motif sequences upon binding to **PBP1** and **PBP2** was further investigated by measuring the donor decay of dual labeled sequences (Fig. S13-S16, ESI). The folding states of the dual labeled sequences were assigned on the basis of the R_{DA} determined from the average lifetime (τ_{avg}) of donor (D) labeled *c-MYC*-C and *BCL-2*-C (τ_D) and donor-acceptor (DA) dual labeled c-MYC-C and *BCL-2*-C (τ_{DA}) i-motif sequences using equation S10 (Table 2 and S7, ESI). The free *BCL-2*-C i-motif sequence at pH 7 exhibited a R_{DA} value of ~ 52 Å, which was decreased to ~ 43 Å for the folded *BCL-2*-C (pH 4.8). A similar decrease in R_{DA} value was observed for the free *c-MYC*-C i-motif sequence upon decreasing the pH from 7 (R_{DA} ~ 54.3 Å) to 4.8 (R_{DA} ~ 44 Å). As observed in smFRET, the R_{DA} values of the free *BCL-2*-C and *c-MYC*-C i-motif sequences were decreased to ~ 40 Å and ~ 47 Å, respectively upon binding to **PBP1,** at pH 7 (Table 2). However, no sharp decrease in R_{DA} values was observed after addition of **PBP2** to *BCL-2*-C and *c-MYC*-C i-motif sequences at pH 7.

Conversely, the addition of **PBP2** decreased the R_{DA} value of free *BCL-2*-G and *c-MYC*-G from ~ 55 Å to ~ 41 Å in the absence of K^+ ions (Table S8, ESI), which indicates that **PBP2** folds single stranded *BCL-2*-G and *c-MYC*-G G-rich sequences into G-quadruplex structures. However, no significant changes in the R_{DA} values of mutant *BCL-2* C-rich and G-rich sequences were noted upon addition of **PBP1** and **PBP2** (Table 2, S8 and Fig. S15, ESI). These results suggest that the observed changes in R_{DA} values of the investigated sequences are due to the formation of folded G-quadruplex or i-motif structures in the presence of ligands.

In agreement with smFRET and lifetime analysis, the CD spectroscopy also supports that the ligand **PBP1** triggers the formation of *BCL-2*-C and *c-MYC*-C i-motif structures and **PBP2** induces the formation of G-quadruplex structures (Fig. S17-S24, ESI). Moreover, the change in CD intensity with the mole fraction of ligands (Job's plot) suggests a 1:1 binding stoichiometry of **PBP1** and **PBP2** with i-motifs and G-quadruplexes, respectively (Fig. S25 and S26, ESI).

Table 2 Lifetime parameters of *BCL-2*-C and *c-MYC*-C i-motifs.

System		τ_{avg}[a]	ε_{FRET}[a]	R_{DA}[a] (Å)
BCL-2-C (pH 7)	D	3.78	0.59	52
	DA	1.56		
[b]*BCL-2*-C-mut (pH 7)	D	3.62	0.53	54
	DA	1.7		
BCL-2-C (pH 4.8)	D	4.32	0.81	43.2
	DA	0.84		
BCL-2-C + **PBP1** (pH 7)	D	3.24	0.87	40.1
	DA	0.42		
BCL-2-C-mut + **PBP1** (pH 7)	D	2.05	0.55	53
	DA	0.92		
BCL-2-C + **PBP2** (pH 7)	D	2.43	0.67	48.9
	DA	0.79		
BCL-2-C-mut + **PBP2** (pH 7)	D	2.34	0.59	52
	DA	0.96		
c-MYC-C (pH 7)	D	3.32	0.52	54.3
	DA	1.6		
c-MYC-C (pH 4.8)	D	4.62	0.79	44.1
	DA	0.97		
c-MYC-C + **PBP1** (pH 7)	D	3.04	0.72	47
	DA	0.87		
c-MYC-C + **PBP2** (pH 7)	D	2.7	0.62	50.7
	DA	1.02		

[a]± 10 %; [b]*BCL-2*-G-mut: 5′-FAM-d(AG_2TGCG_2TCGC $G_2AAG_2A_2G_2$ TG_2 C GTAA GCG_2TGCTG)-TAMRA-3′

Growth inhibition assay

The growth-inhibitory activity of ligands **PBP1** and **PBP2** on human breast adenocarcinoma cells (MCF-7), human colon cancer cells (HCT116) cells and normal mouse myoblast (C2C12) cells were evaluated using MTT assay (Fig. S27 and S28, ESI).[52] After 24 h treatment of cells, **PBP1** showed IC_{50} values of 17.9 ± 1.8 μM and 18.5 ± 1.9 μM in MCF-7 and HCT116 cells, respectively. Ligand **PBP2** displayed IC_{50} values of 3.3 ± 0.7 μM and 3.9 ± 0.9 μM in MCF-7 cells and HCT116 cells, respectively after 24 h (Table S9, ESI). The IC_{50} values suggested a differential effect of **PBP1** and **PBP2** on cancer cells after 48 h treatment**.** When the cells were treated with **PBP1** for 48 h, no significant change in IC_{50} values (14.4 ± 1.4 μM for MCF-7 and 15.1 ± 1.5 μM for HCT116 cells) were observed (Fig. S28 and Table S10, ESI). However, treatment of cells with **PBP2** for 48 h caused a nearly 10 fold decrease in IC_{50} values (1.7 ± 0.2 μM for MCF-7 and 1.3 ± 0.15 μM for HCT116 cells) as compared to **PBP1**. This indicates that **PBP2** can considerably inhibit the growth of cancer cells after 48 h treatment while **PBP1** shows less potent cytotoxic activity. Importantly, both **PBP1** and **PBP2** exhibited negligible toxicity towards normal C2C12 cells after 48 h treatment even at >40 μM concentration.

Ligand-dependent *BCL-2* expression in cancer cells

(a) qRT-PCR analysis. To investigate the ability of **PBP1** and **PBP2** to regulate the expression of *BCL-2* gene in biological

View Article Online
DOI: 10.1039/C7SC02693E

system, we measured the level of *BCL-2* expression at transcriptional and translational levels. After 24 h treatment with IC_{50} dose (24 h) of **PBP1** and **PBP2**, the total RNA was isolated from MCF-7 and HCT116 cells. The level of transcription of the *BCL-2* was quantified using qRT-PCR. Gene expression was normalized against the expression of constitutively expressed house-keeping gene, glyceraldehyde-3-phosphate dehydrogenase (GAPDH). Treatment with the **PBP2** reduced *BCL-2* mRNA level to 0.3-fold (by 70 %) and 0.24-fold (by 76 %) in MCF-7 and HCT116 cells, respectively compared to the control (Fig. 4a and Table S14, ESI). In contrast, when cells were treated with **PBP1**, the *BCL-2* mRNA expression was upregulated to 1.45-fold (by 45 %) and 1.35-fold (by 35 %) in MCF-7 and HCT116 cells, respectively compared to the control (Fig. 4a and Table S12, ESI). In addition to GAPDH, gene expression was also normalized using 18S rRNA as a control gene (Fig. S29, ESI). Treatment with IC_{50} dose (24 h) of **PBP1** upregulated *BCL-2* mRNA level to 1.5-fold (by 50 %), whereas treatment with IC_{50} dose (24 h) of **PBP2** reduced *BCL-2* mRNA level to 0.13-fold (by 87 %) with respect to the 18S rRNA control in HCT116 cells (Table S11 and S13, ESI). However, the GAPDH mRNA and 18S rRNA was equally expressed in the untreated control and ligand treated MCF-7 and HCT116 cells, indicating the gene specific behaviour of the bis-prolinamide derivatives.

(b) Western blot analysis. Having assessed the expression of *BCL-2* at the transcriptional level, we employed western blot analysis to observe the effect of these ligands at the translational level (Fig. 4b, 4c and Fig. S30, ESI). Protein levels of the *BCL-2* and GAPDH were measured in MCF-7 and HCT116 cells treated with **PBP1** and **PBP2** for 24 h at their respective IC_{50} doses (24 h). The western blots exhibited differential effect of **PBP1** and **PBP2** on the expression of *BCL-2* compared to the control cells, which is in good agreement with the qRT-PCR analysis data. The protein expressions calculated from densitometric analysis of western blots were normalized for ligand treated cells against untreated control cells. In **PBP2** treated MCF-7 and HCT116 cells, *BCL-2* protein expression was downregulated by 70 % and 85 %, respectively (Fig. 4c). In contrast, *BCL-2* protein was upregulated by 40 % and 50 % in **PBP1** treated MCF-7 and HCT116 cells, respectively. On the other hand, negligible reduction in GAPDH expression was observed in both treated and control cells. These results suggest that the *meta*-prolinamide **PBP2** can downregulate the *BCL-2* expression, whereas the treatment of *para*-prolinamide **PBP1** results in upregulation of the *BCL-2* expression at both mRNA and protein levels in cancer cells.

(c) Dual-luciferase assay. In order to investigate the influence of the ligands (**PBP1** and **PBP2**) on the *BCL-2* gene expression, we employed dual-luciferase reporter assay (Scheme 2 and Fig. 4d). Reporter vectors containing wild-type *BCL-2* promoter sequences (i-motif and G-quadruplex forming sequences) in the upstream region of firefly luciferase coding gene (LB322) were co-transfected with *Renilla* luciferase vector containing non G- or C-rich promoter sequence (pRL-TK) into HCT116 cells. After cellular uptake of the reporter luciferase vectors, 5 μM of **PBP1** or **PBP2** were added to the cells. As expected, the *Renilla* luciferase expression was unaffected by ligands due to the absence of C-rich or G-rich sequences. Hence, the expression of *BCL-2* firefly luciferase was normalized relative to the *Renilla* luciferase expression.

Upon treatment with **PBP2**, the *BCL-2* promoter-linked luciferase expression was decreased by 58 % relative to the untreated control. In contrast, treatment with **PBP1** exhibited a 42 % increase in *BCL-2* promoter-linked luciferase expression compared to the control. To further validate our results, we also investigated the effect of **PBP1** and **PBP2** on a firefly luciferase vector (pBV-Luc) containing non i-motif or G-quadruplex sequence (Fig. S31, ESI). Interestingly, we did not observe any notable change in firefly luciferase expession in pBV-Luc treated HCT116 cells upon treatment of **PBP1** and **PBP2** compared to untreated control. In addition, ligand **PBP1** did not show any significant change in the expression of reporter vector containing other promoter i-motif or G-quadruplex forming sequences such as *c-MYC* (Del 4 plasmid, Fig. S32, ESI). These results indicate that **PBP1** and **PBP2** may regulate *BCL-2* expression by targeting *BCL-2* promoter i-motifs or quadruplexes in cancer cells.

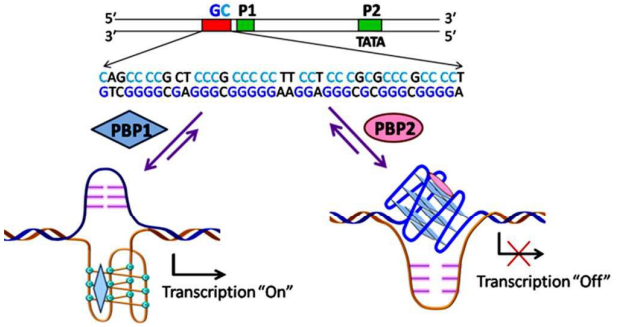

Scheme 2 Schematic representation of the working hypothesis: *BCL-2* GC-rich promoter region forming G-quadruplexes and i-motifs in opposite strands in presence of the peptidomimetic ligands **PBP1** and **PBP2**.

Detection of Apoptosis by Annexin V and Caspases 3/7

To further investigate the influence of bis-prolinamides on cell survival, flow cytometry was employed using Annexin V and PI dual staining assay (Fig. 4e and S33, ESI). Since **PBP1** did not influence the healthy cancer cells in apoptosis assay (unpublished data), we prepared model apoptotic cells by 48 h serum starvation to investigate the antiapoptotic properties.[53] MCF-7 and HCT116 cells were treated with 5 μM **PBP1** and **PBP2** after serum starvation. Control MCF-7 cells show a significant percent of apoptotic cells (~ 22 %) due to serum starvation. Interestingly, treatment with **PBP1** reduced the percent of apoptotic MCF-7 cells to ~ 14 % whereas **PBP2** efficiently increased the percent of apoptotic MCF-7 cells to ~ 60 %. Similar results were obtained for **PBP1** and **PBP2** treated HCT116 cells (Fig. S33, ESI).

Since activation of caspases is an important process during apoptosis, the quantitative detection of executioner caspases 3 and 7 in HCT116 cells upon treatment of peptidomimetic

View Article Online
DOI: 10.1039/C7SC02693E

ligands **PBP1** and **PBP2** was investigated using FLICA reagent based flow cytometry assay (Fig. S34 and Table S15, ESI).[54] The serum starved control cells exhibited moderate levels of active caspases 3 and 7 (~ 18.4 %). At 24 h post treatment of ligand **PBP1** (5 μM), the level of active caspases 3/7 was significantly decreased (~ 5.1 %). However, cells incubated with ligand **PBP2** (5 μM) for 24 h exhibited a higher level of active caspases 3/7 (~ 44.7 %). These results suggest that **PBP1** decreases the level of active caspases 3 and 7 in cancer cells whereas **PBP2** induced apoptosis is associated with the activation of caspases 3 and 7. However, the exact molecular mechanism of this behaviour is under investigation.

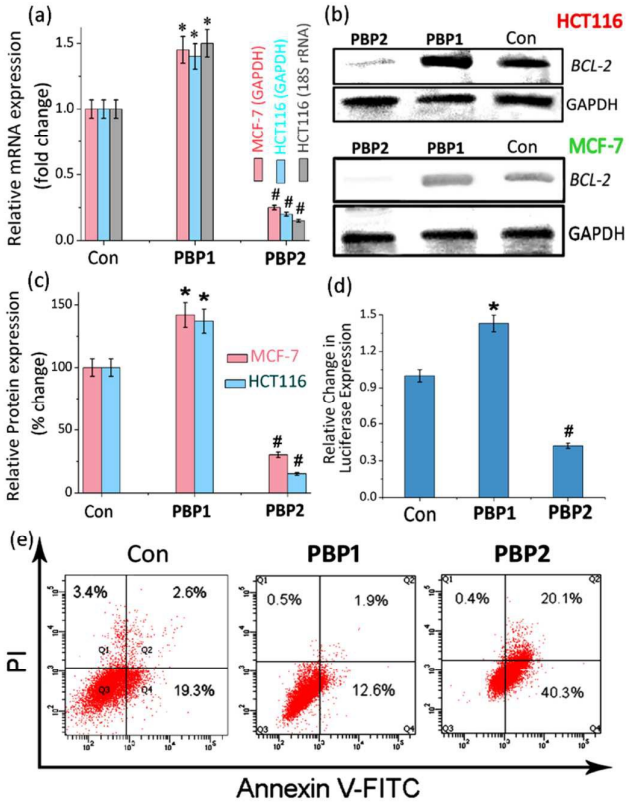

Fig. 4 (a) Determination of transcriptional regulation of *BCL-2* mRNA in the presence of IC_{50} doses (24 h) of **PBP1** or **PBP2** in cancer cells (MCF-7 and HCT116) by qRT-PCR and quantified by double delta C_t analysis using GAPDH and 18S rRNA as reference genes. Data is presented in terms of fold change (the expression of control is 1 fold). The data are shown as mean ± SD. *P < 0.05, #P < 0.01, versus untreated cancer cells; (b) Immunoreactive bands of *BCL-2* protein were analyzed by Western blot in MCF-7 and HCT116 cells. The data are shown as mean ± SD. *P < 0.05, #P < 0.01, versus untreated cancer cells; (c) The protein expression of *BCL-2* protein in the presence of IC_{50} doses (24 h) of **PBP1** or **PBP2** in MCF-7 and HCT116 cancer cells; (d) Relative luciferase expression in LB322 *BCL-2* promoter containing firefly plasmid normalized with pRL-TK Renilla plasmid (FF/RL) upon treatment of 5 μM of **PBP1** and **PBP2** in HCT116 cells, Data shown here as mean ± SD. *P < 0.05, #P < 0.01, versus untreated cancer cells; (e) Flow cytometric analysis upon treatment of 5 μM of **PBP1** and **PBP2** in serum starved MCF-7 cells, Q3, Q4, Q2, and Q1 indicate healthy cells, early, late apoptotic, and necrotic cells, respectively.

Conclusion

We have demonstrated that two flexible peptidomimetic congeners **PBP1** and **PBP2**, synthesized using 'Click Chemistry' can exhibit distinguishable recognition between i-motifs and G-quadruplexes. FRET melting and fluorescence spectroscopic studies reveal that both ligands show high selectivity for i-motifs and G-quadruplexes over duplex DNA. These studies also indicate that **PBP1** preferentially binds to *BCL-2*-C i-motif over G-quadruplexes and **PBP2** selectively binds to G-quadruplexes over i-motifs. In addition, smFRET studies indicate that **PBP1** folds the unstructured *BCL-2* and *c-MYC* C-rich DNA sequences into i-motif structures at neutral pH; whereas **PBP2** promotes G-quadruplex formation from single stranded *BCL-2* and *c-MYC* G-rich sequences in the absence of metal ions. Cellular studies revealed that **PBP1** upregulates *BCL-2* gene expression while **PBP2** inhibits *BCL-2* gene expression. Furthermore, **PBP2** triggers apoptosis by activation of caspases 3 and 7; whereas **PBP1** reduces the level of active caspases 3/7 and decreases the percentage of apoptotic cancer cells. These results indicate that a small change in the ligand structure can bring a dramatic effect on the molecular recognition properties, providing a new platform to achieve differential recognition of G-quadruplexes and i-motifs. These observations further suggest that ligand induced folding of i-motifs or G-quadruplexes may provide an attractive way to control gene expression and to develop therapeutics for cancer and neurodegenerative diseases.

Acknowledgment

The authors thank Professor Shankar Balsubramanian for useful suggestions. We thank DST, India and DST-Center for Ultrafast Spectroscopy and Microscopy for funding. KB thanks DST for a JC Bose fellowship. JD thanks DST for a SwarnaJayanti fellowship and DBT for funding. MD and RP thanks DST for an INSPIRE fellowship and SG thanks CSIR-India for research fellowship. We thank Dr Tania Das, Dr Y. Pavan Kumar and Gargi Chakraborti for their help during the preparation of the manuscript.

References

1 K. Gehring, J. L. Leroy and M. Gueron, *Nature*, 1993, **363**, 561-565.
2 M. L. Bochman, K. Paeschke and V. A. Zakian, *Nat. Rev. Genet.*, 2012, **13**, 770-780.
3 K. Guo, A. Pourpak, K. Beetz-Rogers, V. Gokhale, D. Sun and L. H. Hurley, *J. Am. Chem. Soc.*, 2007, **129**, 10220-10228.
4 C. Chen, M. Li, Y. Xing, Y. Li, C.-C. Joedecke, J. Jin, Z. Yang and D. Liu, *Langmuir*, 2012, **28**, 17743-17748.
5 S. Dhakal, Z. Yu, R. Konik, Y. Cui, D. Koirala and H. Mao, *Biophys. J.*, 2012, **102**, 2575-2584.
6 Y. Cui, D. Kong, C. Ghimire, C. Xu and H. Mao, *Biochemistry*, 2016, **55**, 2291-2299.
7 T. A. Brooks and L. H. Hurley, *Nat. Rev. Cancer*, 2009, **9**, 849-861.
8 G. F. Salgado, C. Cazenave, A. Kerkour and J.-L. Mergny, *Chem. Sci.*, 2015, **6**, 3314-3320.
9 K. M. Felsenstein, L. B. Saunders, J. K. Simmons, E. Leon, D. R. Calabrese, S. Zhang, A. Michalowski, P. Gareiss, B. A. Mock and J. S. Schneekloth, *ACS Chem. Biol.*, 2016, **11**, 139-148.

View Article Online
DOI: 10.1039/C7SC02693E

10 D. Sun and L. H. Hurley, *J. Med. Chem.*, 2009, **52**, 2863-2874.
11 R. Rodriguez, S. Müller, J. A. Yeoman, C. Trentesaux, J.-F. Riou and S. Balasubramanian, *J. Am. Chem. Soc.*, 2008, **130**, 15758-15759.
12 A. Siddiqui-Jain, C. L. Grand, D. J. Bearss and L. H. Hurley, *Proc. Natl. Acad. Sci. U. S. A.*, 2002, **99**, 11593-11598.
13 B. Maji and S. Bhattacharya, *Chem. Commun.*, 2014, **50**, 6422-6438.
14 D. Panda, M. Debnath, S. Mandal, I. Bessi, H. Schwalbe and J. Dash, *Sci. Rep.*, 2015, **5**, 13183.
15 G. W. Collie and G. N. Parkinson, *Chem. Soc. Rev.,* 2011, **40**, 5867-5892.
16 S. Balasubramanian, L. H. Hurley and S. Neidle, *Nat. Rev. Drug Discov.*, 2011, **10**, 261-275.
17 J. Alzeer, B. R. Vummidi, P. J. C. Roth and N. W. Luedtke, *Angew. Chem. Int. Ed.*, 2009, **48**, 9362.
18 S. Kendrick, H.-J. Kang, M. P. Alam, M. M. Madathil, P. Agrawal, V. Gokhale, D. Yang, S. M. Hecht and L. H. Hurley, *J. Am. Chem. Soc.*, 2014, **136**, 4161-4171.
19 H.-J. Kang, S. Kendrick, S. M. Hecht and L. H. Hurley, *J. Am. Chem. Soc.*, 2014, **136**, 4172-4185.
20 B. Roy, P. Talukder, H.-J. Kang, S. S. Tsuen, M. P. Alam, L. H. Hurley and S. M. Hecht, *J. Am. Chem. Soc.* 2016, **138**, 10950-10962.
21 H. A. Day, P. Pavlou and Z. A. E. Waller, *Bioorg. Med. Chem.*, 2014, **22**, 4407-4418.
22 E. P. Wright, H. A. Day, A. M. Ibrahim, J. Kumar, L. J. E. Boswell, C. Huguin, C. E. M. Stevenson, K. Pors and Z. A. E. Waller, *Sci. Rep.*, 2016, **6**, 39456.
23 P. V. Jena, P. S. Shirude, B. Okumus, K. Laxmi-Reddy, F. Godde, I. Huc, S. Balasubramanian and T. Ha, *J. Am. Chem. Soc.*, 2009, **131**, 12522-12523.
24 S. Weiss, *Science,* 1999, **283**, 1676-1683.
25 A. A. Deniz, M. Dahan, J. R. Grunwell, T. Ha, A. E. Faulhaber, D. S. Chemla, S. Weiss and P. G. Schultz, *Proc. Natl. Acad. Sci. U. S. A.*, 1999, **96**, 3670-3675.
26 L. Ying, J. J. Green, H. Li, D. Klenerman and S. Balasubramanian, *Proc. Natl. Acad. Sci. U. S. A.,* 2003, **100**, 14629-14634
27 T. Ha, *Nat. Meth.,* 2014, **11**, 1015-1018
28 P. S. Shirude, B. Okumus, L. Ying, T. Ha and S. Balasubramanian, *J. Am. Chem. Soc.,* 2007, **129**, 7484-7485.
29 J. Choi and T. Majima, *Chem. Soc. Rev.,* 2011, **40**, 5893-5909.
30 J. Choi and T. Majima, *Photochem. Photobiol.,* 2013, **89**, 513-522.
31 S. L. Noer, S. Preus, D. Gudnason, M. Aznauryan, J.-L. Mergny and V. Birkedal, *Nucleic Acids Res.*, 2016, **44**, 464-471.
32 T. Otosu, K. Ishii and T. Tahara, *Nat. Commun.,* 2015, **6**, 7685.
33 A. Tanaka, J. Choi, S. K. Kim and T. Majima, *J. Phys. Chem. B*, 2013, **117**, 6711-6717.
34 M. Debnath, S. Ghosh, D. Panda, I. Bessi, H. Schwalbe, K. Bhattacharyya and J. Dash, *Chem. Sci.,* 2016, **7**, 3279-3285.
35 S. Dhakal, J. D. Schonhoft, D. Koirala, Z. Yu, S. Basu and H. Mao, *J. Am. Chem. Soc.*, 2010, **132**, 8991-8997.
36 Y. Cui, D. Koirala, H. Kang, S. Dhakal, P. Yangyuoru, L. H. Hurley and H. Mao, *Nucleic Acids Res.*, 2014, **42**, 5755-5764.
37 J. Choi, S. Kim, T. Tachikawa, M. Fujitsuka and T. Majima, *J. Am. Chem. Soc.*, 2011, **133**, 16146-16153.
38 A. Grauer and B. König, *Eur. J. Org. Chem.*, 2009, **2009**, 5099-5111.
39 Y. L. Angell and K. Burgess, *Chem. Soc. Rev.*, 2007, **36**, 1674-1689.
40 A. H. El-Sagheer and T. Brown, *Chem. Sci.*, 2014, **5**, 253-259.
41 A. D. Moorhouse, A. M. Santos, M. Gunaratnam, M. Moore, S. Neidle and J. E. Moses, *J. Am. Chem. Soc.*, 2006, **128**, 15972-15973.
42 W. C. Drewe and S. Neidle, *Chem. Commun.*, 2008, 5295-5297.
43 A. D. Moorhouse, S. Haider, M. Gunaratnam, D. Munnur, S. Neidle and J. E. Moses, *Mol. BioSyst.*, 2008, **4**, 629-642.
44 E. P. Wright, J. L. Huppert and Z. A. E. Waller, *Nucleic Acids Res.,* 2017, **45**, 2951-2959.
45 A. M. Fleming, Y. Ding, R. A. Rogers, J. Zhu, J. Zhu, A. D. Burton, C. B. Carlisle and C. J. Burrows, *J. Am. Chem. Soc.*, 2017, **139**, 4682-4689.
46 J.-L. Mergny, *Biochemistry*, 1999, **38**, 1573-1581.
47 H. A. Day, C. Huguin and Z. A. E. Waller, *Chem. Commun.*, 2013, **49**, 7696-7698.
48 J. Dai, E. Hatzakis, L. H. Hurley and D. Yang, *PLoS ONE*, 2010, **5**, e11647.
49 D. Monchaud and M.-P. Teulade-Fichou, *Methods Mol. Biol., Humana Press, Totowa, NJ*, 2010, 257-271.
50 Q. Sheng, J. C. Neaverson, T. Mahmoud, C. E. M. Stevenson, S. E. Matthews and Z. A. E. Waller, *Org. Biomol. Chem.*, 2017, **15**, 5669-5673.
51 D. D. Le, M. Di Antonio, L. K. M. Chan and S. Balasubramanian, *Chem. Commun.*, 2015, **51**, 8048-8050.
52 T. Mosmann, *J. Immunol. Methods*, 1983, **65**, 55-63.
53 A. J. Raffo, H. Perlman, M.-W. Chen, M. L. Day, J. S. Streitman and R. Buttyan, *Cancer Res.*, 1995, **55**, 4438-4445.
54 C. Slator, N. Barron, O. Howe and A. Kellett, *ACS Chem. Biol.*, 2016, **11**, 159-171.

View Article Online
DOI: 10.1039/C7SC02693E

TOC: Ligand-dependent regulation of gene expression has been delineated by targeting i-motifs and G-quadruplexes.